ELSEVIER

Journal of Nuclear Materials 301 (2002) 81–89

journal of nuclear materials

www.elsevier.com/locate/jnucmat

Effects of annealing on tensile property and corrosion behavior of Ti–Al–Zr alloy

Tae-Kyu Kim *, Byung-Seon Choi, Yong-Hwan Jeong, Doo-Jeong Lee, Moon-Hee Chang

Korea Atomic Energy Research Institute, P.O. Box 105, Yuseong, Daejeon 305-600, South Korea

Received 16 July 2001; accepted 22 December 2001

Abstract

The effects of annealing on the tensile property and corrosion behavior of Ti–Al–Zr alloy were evaluated. The annealing in the temperature range from 500 to 800 °C for 1 h induced the growth of the grain and the precipitate sizes. The results of tensile tests at room temperature showed that the strengths and the ductility were almost independent of the annealing temperature. However, the results of corrosion test in an ammonia aqueous solution of pH 9.98 at 360 °C showed that the corrosion resistance depended on the annealing temperature, and the corrosion rate was accelerated with increasing annealing temperature. Hydrogen contents absorbed during the corrosion test of 220 days also increased with the annealing temperature. It could be attributed to the growth of Fe-rich precipitates by annealing. It is thus suggested that the lower annealing temperatures provide the better corrosion properties without degrading the tensile properties.

PACS: 81.65.Mq; 28.41.Qb

1. Introduction

Titanium alloys have drawn wide attention as candidate materials for heat-exchange tubes in steam generators in a small-sized advanced integral pressurized water reactor (PWR) due to their excellent corrosion resistance, good mechanical properties, attractive low density, and suitable durability characteristics [1–8]. Because the heat-exchange tubes are exposed to the primary coolant water at high temperatures and in high-pressure environments, an excellent corrosion resistance is required for safe operation for long periods.

In the manufacturing processes of the heat-exchange tube, the extruded, and mill-annealed titanium alloy tubes are usually subjected to cold working for their coiling. The plastically deformed tubes should be annealed to relieve the stress from the cold working. The annealing temperature thus became a subject of main concern. However, there has been little indication that the annealing temperature reveals any significant effects on the tensile properties and corrosion behavior of titanium alloys.

The purpose of this study is to evaluate the effects of annealing on the tensile property and corrosion behavior of Ti–Al–Zr alloy.

2. Experimental procedure

Ti–Al–Zr alloy tubes (6 mm OD × 4 mm ID) were prepared in extruded and mill-annealed conditions. The chemical composition is given in Table 1. The alloy tubes were annealed in a high vacuum in the temperature range from 500 to 800 °C for 1 h, and then water quenched.

Tensile specimens with a gauge length of 50 mm were prepared. Room temperature tensile tests were

* Corresponding author. Tel.: +82-42 868 2522; fax: +82-42 862 0432.

E-mail address: ex-kimtk@kaeri.re.kr (T.-K. Kim).

0022-3115/02/$ - see front matter
PII: S0022-3115(02)00710-9

Table 1
Chemical composition of Ti–Al–Zr alloy (wt%)

Ti	Al	Zr	V	Fe	Co	S	C	O	N	H
95.24	2.25	2.24	0.06	0.05	0.14	0.0001	0.0090	0.0050	0.0004	0.0047

performed at a constant crosshead speed of 0.127 mm/s. The Vickers hardness tests were also carried out. Corrosion behavior was evaluated in an ammonia aqueous solution adjusted to pH 9.98 at 360 °C under a pressure of 18.5 MPa for 220 days using a circulating loop system. The water chemistries in the inlet of heating zone (autoclave) were constantly controlled to be about 20 μg/l of dissolved oxygen, 0.2 μg/l of dissolved hydrogen, and 220 μS/l of conductivity. The corrosion kinetics were determined by the gravimetric method.

The microstructures were examined using a transmission electron microscope (TEM)/energy dispersive spectroscope (EDS). Fractured surfaces of the samples after the tensile tests were examined using a scanning electron microscope (SEM). The crystal structures of oxide scales formed on the surfaces of the samples during the corrosion test were studied using X-ray diffraction (XRD) in the scanning range of $2\theta = 20$–$60°$ at a low grazing angle of 3°. The SEM/EDS studies on the oxide surface in the metal–oxide interface were also carried out.

3. Results and discussion

3.1. Microstructure

Fig. 1 shows a bright field TEM image of the longitudinal section of the as-received Ti–Al–Zr alloy tube. The as-received alloy reveals the equiaxed grains with an average grain size of about 20 μm. The crystal structure is identified as a hexagonal close-packed (hcp, $a = 0.2950$ nm, $c = 0.4686$ nm) α-titanium alloy.

Fig. 2 shows TEM/EDS studies on the matrix and precipitates of Ti–Al–Zr alloy. Two kinds of Fe-rich precipitates with the chemical formulations of TiFe (sc, $a = 0.2976$ nm) and $TiFe_2$ (hcp, $a = 0.4785$ nm, $c = 0.7799$ nm) are observed. Most of the precipitates are the TiFe-type phase (Fig. 2(a)). They are usually found in the grains, but occasionally in the grain boundaries. The chemical composition of the TiFe-type phase is determined to be (wt%) 92.04Ti, 2.62Al, 4.36Zr, and 0.98Fe, whereas that of the matrix is analyzed to be (wt%) 93.90Ti, 2.16Al, 3.87Zr, and 0.07Fe. The precipitates of the $TiFe_2$-type phase are occasionally detected in the grain boundaries (Fig. 2(e)), and their chemical composition is determined to be (wt%) 90.30Ti, 1.35Al, 4.60Zr, and 3.75Fe. In fact, the solubility of Fe in titanium alloy reveals to be extremely low [9], and Al is well known as an α-stabilizer element [10].

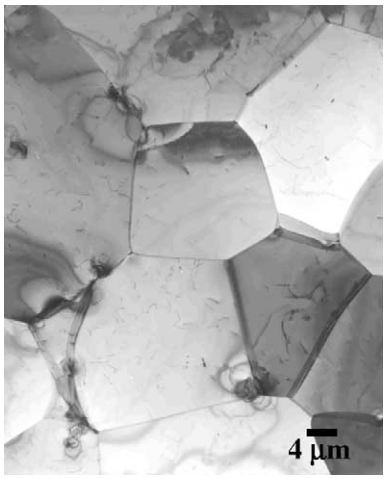

Fig. 1. Bright field TEM image of the longitudinal section of the as-received Ti–Al–Zr alloy tube.

Fig. 3 shows the effect of annealing on the grain size of Ti–Al–Zr alloy. It is observed that the grain size increases with increasing annealing temperature, i.e. from 23.8 μm in the as-received condition to 25.3 μm in the sample annealed at 500 °C, and further up to 43.1 μm at 800 °C.

Fig. 4 shows the effect of annealing on the mean size and area fraction of precipitates in Ti–Al–Zr alloy. The mean size and area fraction of precipitates increase with increasing annealing temperature. No remarkable difference in the shapes of precipitates is observed before and after annealing. This observation means that the annealing induces the diffusion of Fe component in the matrix to enlarge the Fe-rich precipitates, and promotes the diffusion rate of Fe in the matrix to the precipitates as the annealing temperature increases.

3.2. Effect of annealing on the tensile property

Fig. 5 shows the effect of annealing on the tensile property of Ti–Al–Zr alloy. It is apparent that the tensile strengths and elongation are almost independent of the annealing temperature up to 800 °C. The tensile strengths at room temperature depend on the grain size and the amount of precipitates; the small grain size and the large number of precipitates increase the strengths since the grain boundaries and precipitates act as obstacles to the dislocation movement in the presence of stress. The annealing of the alloy induces the grain

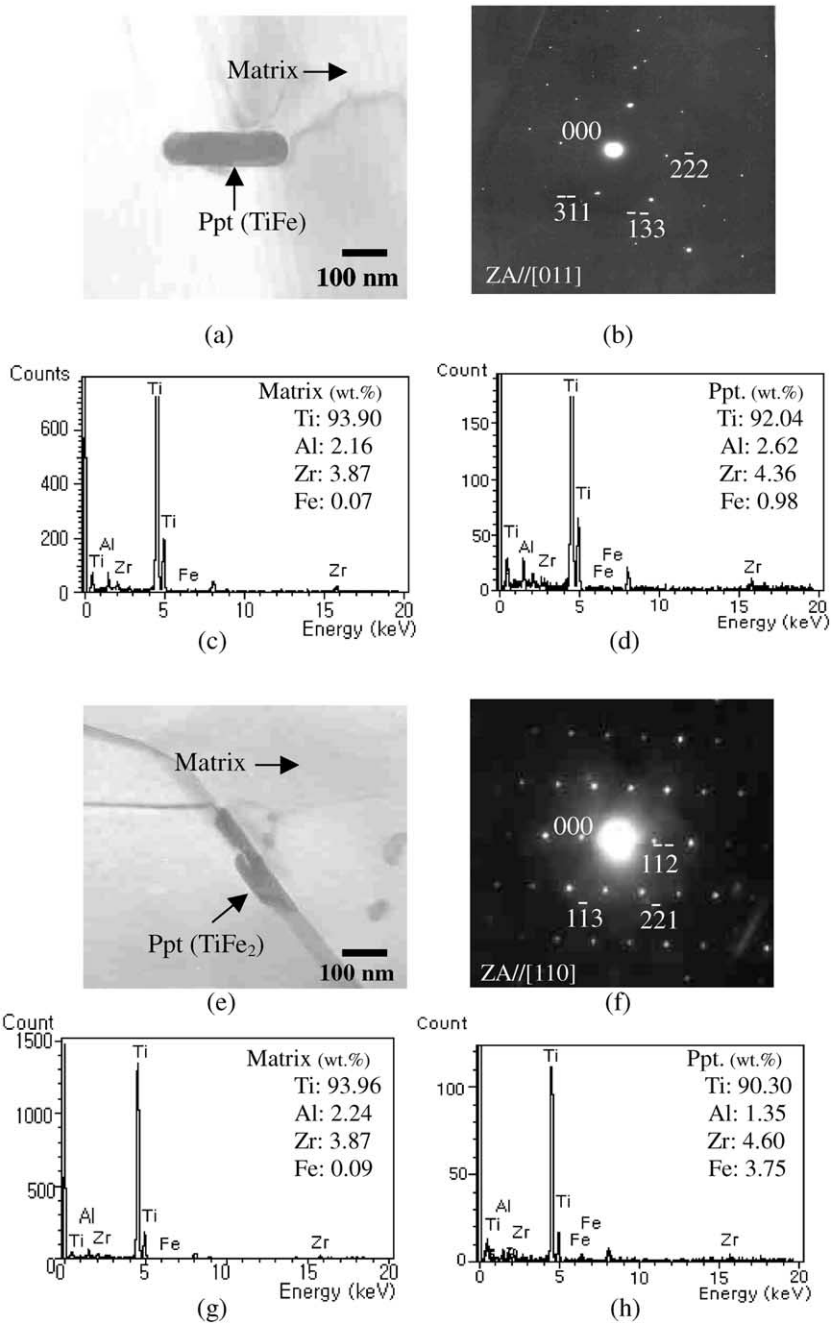

Fig. 2. TEM/EDS results on the matrix and precipitates of Ti–Al–Zr alloy: (a) bright-field image (TiFe), (b) selected area diffraction pattern from precipitation allowed in (a), (c) spectrum from matrix, (d) spectrum from precipitation, (e) bright-field image ($TiFe_2$), (f) selected area diffraction pattern from precipitation allowed in (e), (g) spectrum from matrix, and (h) spectrum from precipitation.

growth (Fig. 3) and the increase in amount of precipitates (Fig. 4). It is thus considered that the decrease in the strengths resulting from the grain growth would be almost compensated by the increase in the strengths resulting from the increase in the number of precipitates, giving little effects of annealing on the tensile properties. These results offer precise knowledge in relation to the effects of annealing on the tensile properties of Ti–Al–Zr alloy.

Fig. 6 shows SEM fractographs after tensile tests of the as-received and of annealed Ti–Al–Zr alloys. The fracture surfaces of the as-received and of annealed

samples are characterized by a ductile fracture. The large dimples are found in the fracture surfaces of both samples, illustrating ductile rupture. The large dimples may be originally intergranular cracks at an early stage of deformation. As deformation proceeds, the original grain boundary cracks may be distorted into the elongated voids, until final failure occurs by necking between the voids, finally forming the dimples. It is concluded that the annealing hardly affects the deformation mechanism of Ti–Al–Zr alloy in the presence of stress at room temperature.

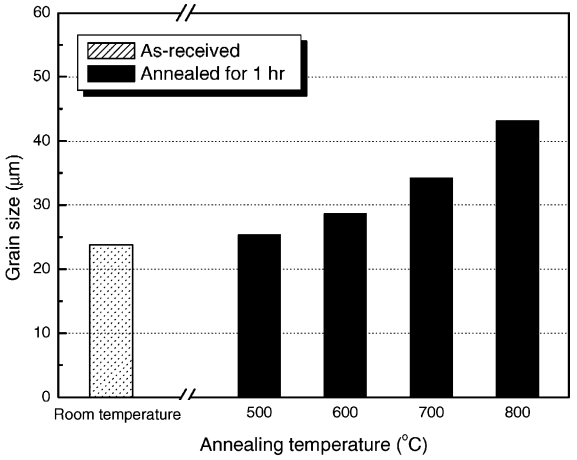

Fig. 3. Effect of annealing on the grain size of Ti–Al–Zr alloy.

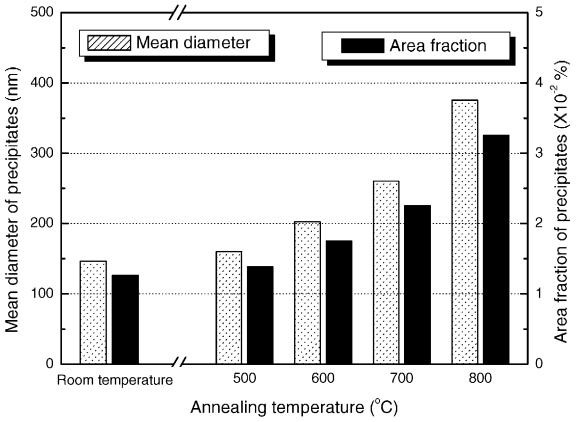

Fig. 4. Effect of annealing on the mean size and area fraction of precipitates in Ti–Al–Zr alloy.

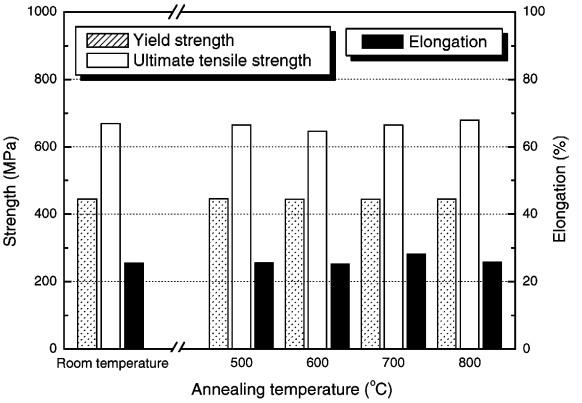

Fig. 5. Effect of annealing on the tensile property of Ti–Al–Zr alloy.

Fig. 7 shows the effect of annealing on the Vickers hardness of Ti–Al–Zr alloy. It is observed that the annealing does not affect the hardness. In fact, the hardness is mainly determined by the grain size and the amount of precipitates; the small grain size and the large amount of precipitates usually increase the hardness. It is considered that the decrease in the hardness resulting from the grain growth would be compensated by the precipitation hardening resulting from the increase in amount of precipitates. These results coincide well with the tensile test results which indicate that there are little effects of annealing on the tensile properties (Fig. 5).

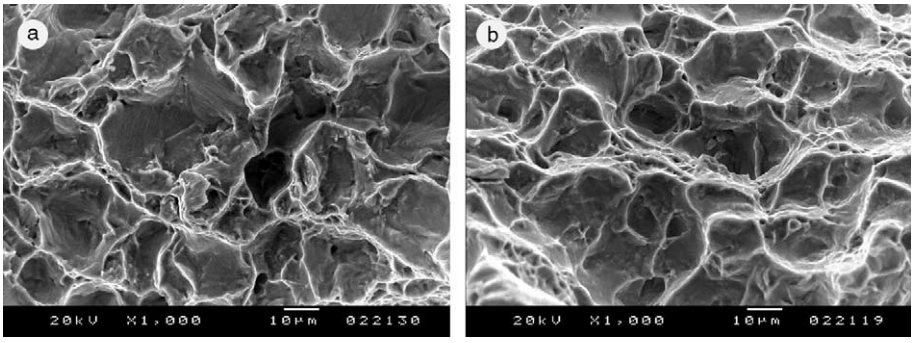

Fig. 6. SEM fractographs after tensile tests of the as-received and of annealed Ti–Al–Zr alloys: (a) as-received, and (b) annealed at 800 °C for 1 h.

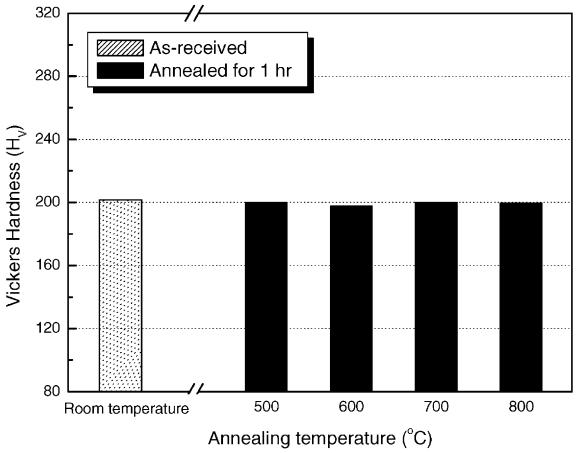

Fig. 7. Effect of annealing on the Vickers hardness of Ti–Al–Zr alloy.

3.3. Effect of annealing on the corrosion behavior

Fig. 8 shows the corrosion behavior of the as-received and of the annealed Ti–Al–Zr alloys in the ammonia aqueous solution of pH 9.98 at 360 °C. The samples with and without annealing exhibit relatively excellent resistance to the corrosion, having the oxide thickness less than 1 μm after the corrosion for 220 days. The excellent corrosion resistance of the alloy is provided by a tenacious oxide layer formed on its surface as a result of an oxidation of titanium with oxygen. The corrosion rate is rapid in the initial corrosion period, but decrease greatly after approximately 60 days. This is closely correlated with the increase in the thickness of a protective oxide layer.

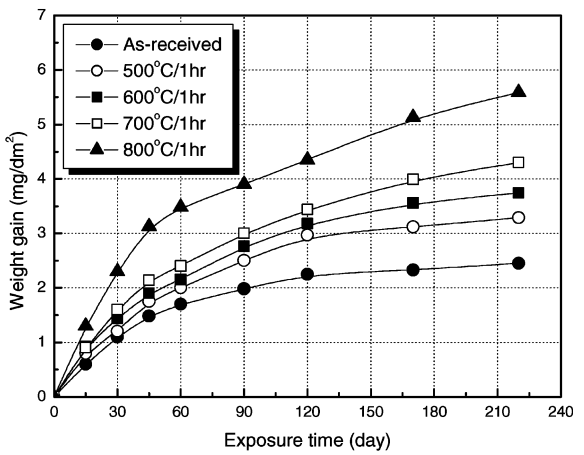

Fig. 8. Corrosion behavior of the as-received and of the annealed Ti–Al–Zr alloys in the ammonia aqueous solution of pH 9.98 at 360 °C.

Fig. 9 shows the XRD patterns of the oxide scales formed on the surfaces of the as-received Ti–Al–Zr alloy corroded in the ammonia water chemistry of pH 9.98 at 360 °C. The peaks of pure Ti appear in the XRD patterns, since the depth of penetration of the X-ray is greater than the thickness of the oxide scale. The several phases of titanium oxide, Ti_2O, TiO, α-$Ti_{1-x}O$, and anatase-TiO_2, are observed on the oxide scale formed during corrosion for 7 days (Fig. 9(a)). This observation

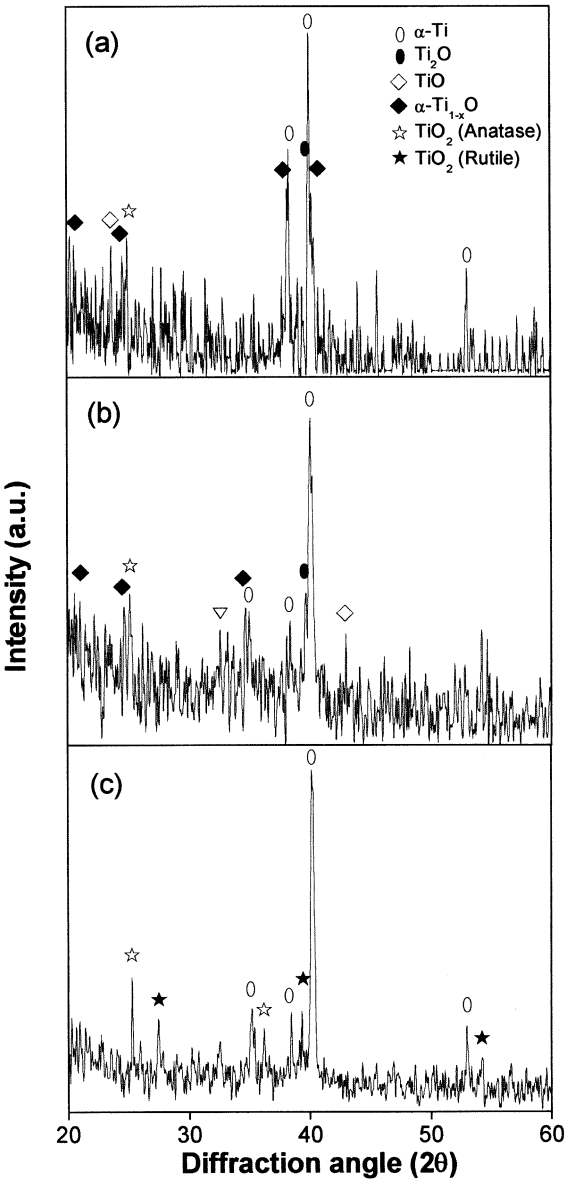

Fig. 9. XRD patterns of the oxide scales formed on the surfaces of the as-received Ti–Al–Zr alloy corroded in the ammonia water chemistry of pH 9.98 at 360 °C for (a) 7, (b) 30, and (c) 120 days.

indicates that the corrosion reaction of Ti follows these steps; Ti → Ti_2O → TiO → α-$Ti_{1-x}O$ → TiO_2. The XRD pattern on the oxide scale formed for 30 days shows a similar tendency with that for 7 days (Fig. 9(b)). As the corrosion further proceeds, the peak of anatase-TiO_2 in the sample corroded for 120 days exhibits to be much higher than those found in the samples corroded for 7 and 30 days (Fig. 9(c)). Even the intermediate phases in the corrosion stages of pure Ti to TiO_2, such as Ti_2O, TiO, and α-$Ti_{1-x}O$, would exist; they are hardly observed since most of the oxide scales compose of TiO_2. The rutile-TiO_2 is also found in the oxide scale (Fig. 9(c)). In fact, the anatase is a metastable phase to be formed in the pressure below about 1380 MPa at 360 °C, while the rutile is a stable phase at all temperatures and ambient pressure [11]. This means that the transformation of anatase to rutile is possible and does not occur reversibly. It is thus considered that the oxide layer formed at early corrosion stage is mainly composed of anatase (Fig. 9(a) and (b)). As the thickness of oxide layer increases, the anatase previously formed is transformed to rutile (Fig. 9(c)).

Fig. 10 shows the effect of annealing on the final weight gains of Ti–Al–Zr alloys after corrosion in the ammonia aqueous solution of pH 9.98 at 360 °C for 220 days. The final weight gains of the samples annealed at 500, 600, 700, and 800 °C appear to be 3.3, 3.7, 4.3, and 5.6 mg/dm^2, respectively, while that of the as-received alloy reveals to be 2.5 mg/dm^2. It is thus obvious that the final weight gains increase with increasing annealing temperature. In other words, the annealing contributes to decrease the corrosion resistance.

Fig. 11 shows the effect of annealing on the corrosion kinetics of Ti–Al–Zr alloy in the corrosion period from 60 to 220 days. It is observed that the slope of the corrosion curve increases with increasing the annealing temperature. This indicates that the annealing accelerates the corrosion rate. It is thus concluded that the lower annealing temperatures provide the better corrosion rates.

3.4. Mechanism of accelerated corrosion by annealing

Fig. 12 shows SEM micrographs and EDS results on the oxide surfaces at the metal–oxide interfaces formed on Ti–Al–Zr alloy annealed at 800 °C. The oxide surface at the metal–oxide interface of the sample corroded for 30 days exhibits a small size of the protruded round oxides in the uniform oxide layer (Fig. 12(a)). For the uniform oxide layer and the protruded oxide allowed in Fig. 12(a), the EDS studies are shown in Fig. 12(b). The protruded oxides contain higher titanium and lower oxygen contents than the uniform oxide layer. If the inside of the protruded oxide contains the un-oxidized precipitates, these observations would be possible. In addition, the protruded oxides always reveal to be higher Fe contents than the uniform oxide layer. These studies indicate that the protruded oxides are correlated with the Fe-rich precipitates. In this aspect, the weight ratio of Fe/Ti would be useful to identify the phase, since it would be little changed before and after corrosion reaction. For the sample annealed at 800 °C, the weight ratios of Fe/Ti in the matrix and precipitates before corrosion are determined to be in the range of 0.036–0.067 and 1.6–4.8, respectively. In the oxide surface, the weight ratios of Fe/Ti in the uniform oxide layer and the protruded round oxide are analyzed to be 0.052 and 4.5, respectively (Fig. 12(b)). It is thus considered that the protruded oxides are mainly composed of the Fe-rich precipitates.

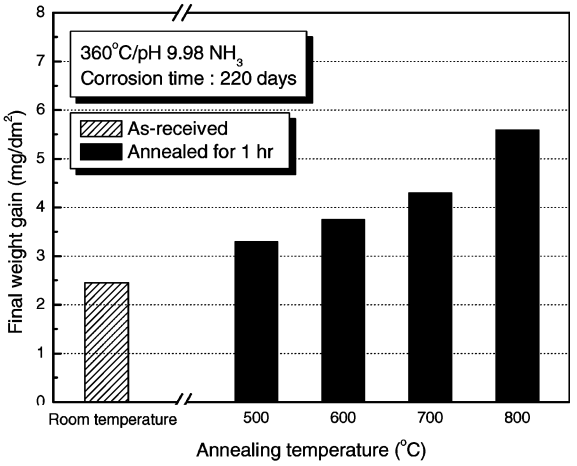

Fig. 10. Effect of annealing on the final weight gain of Ti–Al–Zr alloy after corrosion in the ammonia aqueous solution of pH 9.98 at 360 °C for 220 days.

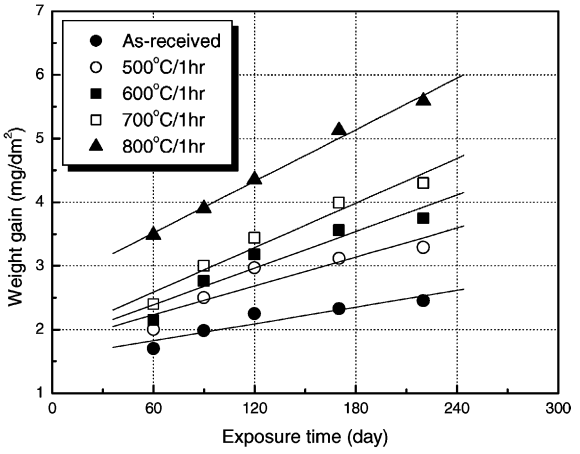

Fig. 11. Effect of annealing on the corrosion kinetics of Ti–Al–Zr alloy in the corrosion period from 60 to 220 days.

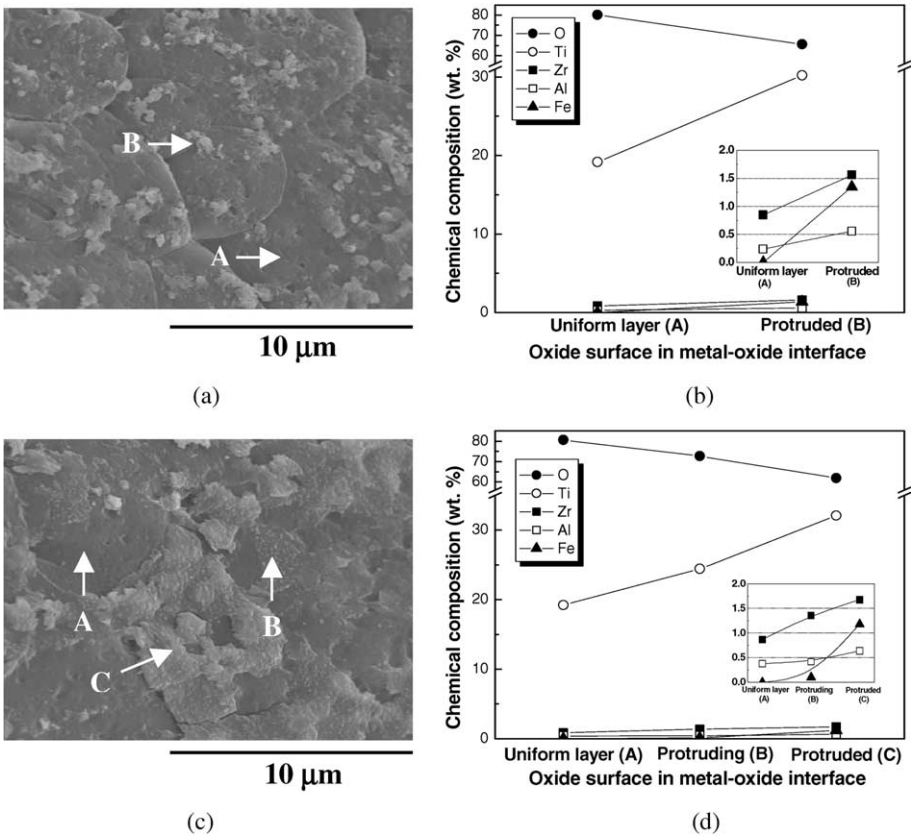

Fig. 12. SEM micrographs and EDS results on the oxide surfaces at the metal–oxide interfaces formed on Ti–Al–Zr alloy annealed at 800 °C: SEM micrographs of exposure time of (a) 30 and (c) 120 days, (b) and (d) EDS results from oxides allowed in (a) and (c), respectively.

As the corrosion proceeds, the surface of oxide layer grown for 120 days exhibits the further growth of the protruded oxides in the uniform oxide layer (Fig. 12(c)). The oxide morphologies can be divided into three district regions; uniform oxide layer, protruding and considerably protruded oxides. The EDS results for three regions allowed in Fig. 12(c) show a similar tendency with those for the oxide surface on the sample corroded for 30 days (Fig. 12(b)); the considerably protruded oxide region contains a large amount of Fe content (Fig. 12(d)), indicating that the protruded oxides are also correlated with the Fe-rich precipitates. The weight ratios of Fe/Ti in the uniform, protruding, and protruded oxide regions are determined to be 0.052, 0.41, and 0.37, respectively. These results are in good agreement with the weight ratios of Fe/Ti in the matrix and precipitates before the corrosion test. Thus, it is believed that the accelerated corrosion by annealing is attributed to the growth of Fe-rich precipitates.

Fig. 13 shows the schematic diagram illustrating the mechanism of accelerated corrosion by the Fe-rich precipitates of Ti–Al–Zr alloy. Based on the SEM/EDS results (Fig. 12), the following prediction would be possible; at first step, the metal–oxide interface would approach the Fe-rich precipitates in the matrix as the corrosion proceeded. When it reached the precipitate (second step), the outer part of precipitate attaching the front of oxide layer would be oxidized. At the same time, the oxygen would diffuse through the metal–precipitate interface, oxidizing the outer part of the precipitate. It was reported that the diffusion rate of Fe in the Fe-rich precipitates of Zr-alloy revealed to be relatively fast than the other elements in the precipitates [12]. Thus, it is considered that the Fe element of the precipitates would diffuse to the matrix–precipitate interface. At third step, the outer part of the precipitate would be oxidized under the high compressive stress produced by the oxidation of the matrix. It is obvious that the oxidation of precipitates would provide the local volume extension by the ratio of Pilling–Bedworth, giving the tensile stress. Near the oxide–precipitate interface, the compressive stress provided by the oxidation of matrix would tend to release, and thus favored to form an equiaxed oxides. In fact, the equiaxed oxides would

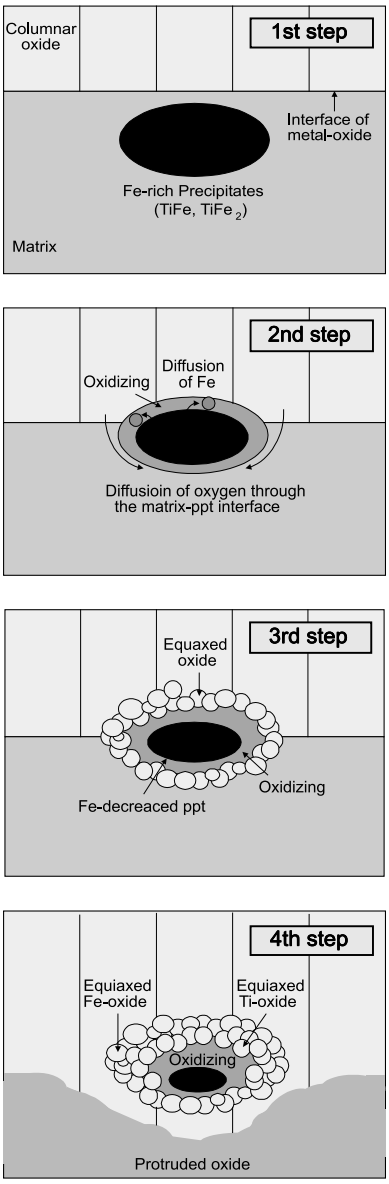

Fig. 13. Schematic diagrams illustrating the corrosion mechanism accelerated by the Fe-rich precipitates of Ti–Al–Zr alloy.

provide easier path to the diffusion of oxygen than the columnar oxides. Finally, the oxidation of precipitates would produce the protruded oxides observed by the SEM/EDS (Fig. 12). As a result, the precipitates in the oxide would act as the additional diffusion path of oxygen (Fig. 13), providing the increase in the corrosion kinetics (Fig. 11). The protruded oxides may also offer the accelerated corrosion rate, since the protruded oxides provide the increase in area of the metal–oxide interface where the corrosion reaction occurs. It is believed that the accelerated corrosion by annealing is attributed

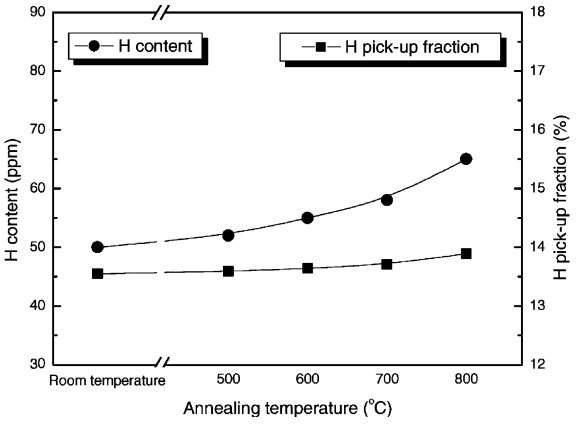

Fig. 14. Hydrogen content and hydrogen pick-up fraction of Ti–Al–Zr alloy after corrosion in the ammonia aqueous solution of pH 9.98 at 360 °C for 220 days.

to the growth of the precipitates that tend to provide the change of crystal structure of oxide from the columnar to the equiaxed, favorable diffusion path of oxygen, and increase in area of the metal–oxide interface.

3.5. Hydrogen pick-up

Fig. 14 shows the hydrogen content and the hydrogen pick-up fraction of Ti–Al–Zr alloys after corrosion in the ammonia aqueous solution of pH 9.98 at 360 °C for 220 days. The hydrogen contents absorbed during corrosion increase with increasing the annealing temperature, i.e. from 3 ppm in the as-received sample to 15 ppm in the sample annealed at 800 °C. The hydrogen contents absorbed during corrosion are correlated with the corrosion resistance; the better corrosion resistance usually provides the lower hydrogen contents absorbed into the metal. In fact, the affinity of Fe-rich precipitates with hydrogen is known to be higher than the matrix [13]. This means that the precipitates in the oxide as illustrated in Fig. 13 would make it easy to diffuse the hydrogen from the ammonia aqueous solution to the metal–oxide interface. As a result, the hydrogen contents absorbed during corrosion increase gradually in proportion to the corrosion resistance as shown in Fig. 10. The hydrogen pick-up fraction is determined to be about 14%. It would be attributed to the characteristics of Ti–Al–Zr alloy during corrosion in the ammonia aqueous solution at 360 °C.

4. Conclusions

In this study, the effects of annealing on the tensile property and corrosion behavior of Ti–Al–Zr alloy for

heat-exchange tubes in steam generators in a small-sized advanced integral PWR were evaluated in order to determine the annealing temperature.

The tensile properties and the hardness at room temperature were almost independent of the annealing temperature, since the annealing in the temperature from 500 to 800 °C induced the growth of the grain size as well as the amount of precipitates. However, the corrosion resistance in the ammonia aqueous solution of pH 9.98 at 360 °C significantly depended on the annealing temperature, and the corrosion rates were accelerated with increasing annealing temperature. Hydrogen contents during the corrosion test for 220 days also increased with the annealing temperature. These corrosion properties could be attributed to the growth of Fe-rich precipitates by annealing. The lower annealing temperatures are suggested to provide the better corrosion properties without degrading the tensile properties at room temperature.

Acknowledgements

The authors would like to express their appreciation to the Ministry of Science and Technology (MOST) of the Republic of Korea for the support of this work through the mid- and long-term nuclear R&D project.

References

[1] O.A. Kozhevnikow, E.V. Nesterova, V.V. Rybin, I.I. Yarmolovich, J. Nucl. Mater. 271 & 272 (1999) 472.
[2] I.V. Gorynin, Mater. Sci. Eng. A 263 (1999) 112.
[3] M.L. Wasz, F.R. Brotzen, R.B. Mclellan, A.J. Griffin Jr., Int. Mater. Rev. 41 (1996) 1.
[4] J.C. Williams, Mater. Sci. Eng. A 263 (1999) 107.
[5] D.G. Kolman, J.R. Scully, J. Electrochem. Soc. 143 (1996) 1847.
[6] E. Rolinski, G. Sharp, D.F. Cowgill, D.J. Peterman, J. Nucl. Mater. 252 (1998) 200.
[7] G. Lutjering, Mater. Sci. Eng. A 263 (1999) 117.
[8] S.V. Gnedenkov, P.S. Gordienko, S.L. Sinebrukhov, O.A. Khrisanphova, T.M. Skorobogatova, Corrosion 56 (2000) 24.
[9] C.J. Smithells (Ed.), Metals Reference Book, 5th Ed., Butterworths, London, 1976, p. 618.
[10] I.M. Poherlyuk, Mater. Sci. 35 (1999) 284.
[11] J.L. Murray, H.A. Wriedt, Bull. Alloy Phase Diagrams 8 (1987) 157.
[12] R. Hahn, J. Nucl. Mater. 245 (1997) 147.
[13] Y. Hatano, K. Isobe, R. Hitaka, M. Sugisaki, J. Nucl. Sci. Tech. 33 (1996) 944.